Diamond & Related Materials 161 (2026) 113154

Contents lists available at ScienceDirect

Diamond & Related Materials

journal homepage: www.elsevier.com/locate/diamond

Mechanical properties and fracture of Net—C18: molecular dynamics study and analytical model

Xintian Cai [a,b,*], Ao Li [c], Xue Chen [c], Zeyu Huang [c,d], Gen Chen [c,d], Chaoyue Ji [e], Han Yan [f], Xiao-Jia Chen [b,*], Qing Peng [b,c,e,*]

[a] School of Mechanical Engineering, Hubei University of Technology, Wuhan, 430068, China
[b] School of Science, Harbin Institute of Technology, Shenzhen, 518055, China
[c] State Key Laboratory of Nonlinear Mechanics, Institute of Mechanics, Chinese Academy of Sciences, Beijing, 100190, China
[d] Institute of Manufacturing Engineering, Huaqiao University, Xiamen, 361021, China
[e] School of Power and Mechanical Engineering, Wuhan University, Wuhan, 430072, China
[f] School of Mechanical and Electrical Engineering, Wuhan University of Technology, Wuhan, 430070, China

ARTICLE INFO

Keywords:
Net-C18
Graphene-like
Molecular dynamics
Mechanical properties

ABSTRACT

Net-C18 is a recently theoretically discovered two-dimensional (2D) carbon allotrope of graphene, and its potential applications in electronics, energy, catalysis, and materials science require further development. Our study aimed to explain the fracture behavior of Net-C18 and the evolution of mechanical properties at the femtosecond and atomic scales. Molecular dynamics simulation methods were used to study the coupling interaction of fracture evolution with temperature, anisotropy, strain rate, pore defects, and random vacancy defects. The results show that the critical strain rate of Net-C18 fracture at 300 K is nearly 0.10 and decreases with the temperature increase, which is about 0.05 at 900 K. The tensile direction, strain rate, voiding, and random vacancy defects significantly affect the mechanical properties. Compared with graphene, Net-C18 is less sensitive to vacancy defects. Notably, intrinsic nanoscale flaws within the material can significantly modify fracture morphology by inducing localized stress concentration and altering crack propagation pathways.

1. Introduction

Graphene-like materials have emerged as a research hotspot in materials science due to their exceptional electronic properties, thermal conductivity, and mechanical performance. Studies have demonstrated that graphene-like materials exhibit ultrahigh electron mobility and superior electrical conductivity [1–3]. Furthermore, their thermal conductivity significantly surpasses that of conventional materials, highlighting their immense potential in thermal management applications [4–6]. Mechanically, graphene-like materials also outperform traditional counterparts in terms of strength and elastic modulus [7]. Unlike graphene, Net-C18 [8] features an alternating arrangement of five-membered, six-membered, and eight-membered rings, which introduces unique mechanical properties. This study aims to elucidate how this structural topology influences the fracture behavior and defect tolerance of Net-C18 compared to other 2D carbon allotropes. Notably, Net—C18, a novel theoretically predicted graphene-like material, is a promising candidate for aerospace, flexible electronics, and composite materials [8]. Consequently, in-depth investigations into the mechanical properties of Net-C18 not only advance materials science but also establish a robust theoretical foundation for practical applications of novel materials [9].

Advanced multimodal characterization techniques, including in situ spectroscopic probing and high-resolution microscopic analyses, serve as the cornerstone for deciphering the atomic-scale mechanisms governing the structural evolution and macroscopic performance of carbon allotropes. For instance, Novoselov et al. first confirmed the existence of graphene through electric field effect experiments, revealing its extraordinary electron mobility [1,10]. Lee et al. employed Raman spectroscopy and nanoindentation techniques to measure graphene's elastic modulus and tensile strength, reporting values of 1 TPa and 130 GPa, respectively [11]. Despite their significance, experimental approaches present notable limitations. First, the high cost and operational complexity of equipment restrict their widespread adoption. Second, experimental outcomes are often influenced by sample preparation protocols and testing conditions, leading to inconsistencies in

* Correspondence to: X. Cai, X.-J. Chen and Q. Peng, School of Science, Harbin Institute of Technology, Shenzhen, 518055, China.
E-mail addresses: caixintian@hbut.edu.cn (X. Cai), xjchen@hit.edu.cn (X.-J. Chen), pengqing@whu.edu.cn (Q. Peng).

https://doi.org/10.1016/j.diamond.2025.113154
Received 10 May 2025; Received in revised form 27 November 2025; Accepted 1 December 2025
Available online 3 December 2025

reproducibility and reliability. In contrast, computational simulations offer distinct advantages in studying graphene-like materials, combining high precision with operational feasibility. These methods enable atomic-scale predictions of material structures and properties while circumventing experimental limitations. Memarian et al. employed molecular mechanics (MM) and density functional theory (DFT) to assess graphene's Young's modulus, systematically comparing the accuracy of computational approaches and establishing theoretical benchmarks for calibrating experimental measurements of nanomechanical properties [12]. Faccio et al. employed molecular dynamics (MD) simulations to explore the influence of doping on the mechanical properties of graphene, uncovering the underlying modulation mechanisms driven by dopant interactions [13].

Among computational methods, MD simulations have garnered significant attention due to their unique capabilities. By numerically integrating Newton's equations of motion under predefined potential energy functions, MD simulations track atomic trajectories to predict mechanical properties. Peng et al. comprehensively reviewed the mechanical properties and applications of graphene-derived materials, emphasizing the critical role of MD simulations in understanding their performance [14,15]. The uniqueness of MD stems from its capacity to resolve non-equilibrium atomic trajectories with thermodynamic irreversibility while capturing microstructure-dependent nonlinear constitutive behavior under finite deformation regimes. For example, Damasceno et al. utilized MD simulations to investigate the impact of vacancy defects on graphene's tensile strength. Their findings indicated that such defects substantially diminish the material's tensile strength [16].

Subsequent studies have further validated the effectiveness of MD simulations. For instance, Mortazavi and Ahzi conducted MD simulations to investigate the thermal conductivity and tensile response of defective graphene. Their findings indicated that the presence of defects significantly reduces both the thermal conductivity and mechanical strength of graphene [17]; Safina et al. conducted a MD study on the mechanical properties and deformation behavior of graphene/metal composites [18]; Zhang et al. conducted a comprehensive review of graphene's fracture behavior, focusing on its fracture strength, fracture toughness, and crack propagation mechanisms [19]; Bhauriyal et al. proposed the potential of a graphene-like carbon–nitride monolayer as an anode material for sodium-ion and potassium-ion batteries [20]; Kumar et al. explored the mechanical properties of graphene, defective graphene, multilayer graphene, and SiC-graphene composites through MD simulations [21]; Santonocito et al. explored recent advancements in graphene-based tunable metasurfaces and their applications in next-generation optical technologies [22]; Yang et al. conducted MD simulations to investigate the thermal conductivity of defective graphene oxide [23]; Anegbe et al. conducted a comprehensive review on the synthesis of graphene oxide (GO) and its applications in the removal of emerging contaminants (ECs) [24]; Akyildiz et al. revisited the challenges of terahertz (THz) band communication and outlined key research directions for the next decade [25]; Rozhkov et al. compared different interatomic potentials for modeling defects in graphene using MD simulations [26]; and Das and Kumar investigated the mechanical properties of aluminum-graphene core-shell nanocomposites using MD simulations [27].

However, these studies overlooked the synergistic effects of combined factors like temperature and defects. Ma et al. investigated the effect of monovacancy defects on the anisotropic mechanical behavior of monolayer graphene using MD simulations [28]. Zhao et al. provided a comprehensive review of the application of MD simulations in studying metal matrix composites (MMCs). Their study highlighted key advances in understanding interfacial interactions, mechanical behavior, and defect evolution in MMCs at the atomic scale [29]. Duhan et al. explored the potential of biphenylene-graphene van der Waals bilayer heterostructures as anode materials for lithium-ion batteries. Their study employed MD simulations to analyze the structural stability, electronic properties, and lithium storage capacity of these heterostructures [30]. Najafi et al. investigated the fatigue resistance of atomically thin graphene oxide using MD simulations and experimental validation [31], while subsequent studies further explored influencing factors and improvement strategies [32–37].

Although previous research provides valuable insights into Net-C18's mechanical behavior, the tensile and fracture behaviors have not been investigated. This study systematically examines the effects of temperature, strain rate, vacancy defects, vacancy defects, anisotropy, and two-dimensional material characteristics on the fracture performance of Net-C18 through MD simulations. By analyzing atomic-scale morphological evolution during fracture processes at femtosecond resolution, we offer a comprehensive understanding of fracture mechanisms. Our approach addresses the limitations of single-factor analyses prevalent in existing literature, establishing a refined theoretical framework for designing and applying graphene-like materials.

2. Materials and methods

2.1. Structural modeling and simulation setup

Net-C18 is a two-dimensional planar crystalline material composed of 18 carbon atoms in a primitive unitcell [8] as displayed in Fig. 1, featuring a unique honeycomb-like structure formed by alternating arrangements of five-membered, six-membered, and eight-membered rings. A super cell contains $64 \times 32 \times 1$ unit-cells was adopted. The orthogonal simulation box has a dimension of $31.45 \times 31.60 \times 10$ nm^3 with periodic boundary conditions applied in the two in-plane directions (x and y directions). For the out-of-plane direction (z-direction), kinematic freedom was preserved to accommodate uniaxial deformation under multiaxial stress states. The x-direction is along the zigzag direction (second nearest-neighbour direction) of the six-membered ring. The y-direction is along the armchair direction (nearest neighbour direction). A vacuum of 10 nm in the out-of-plane direction to reduce the inter-layer interact ions to mimic the single layer nature of Net—C18. The tilt-view of the full model and the top-view of the primitive unitcell are displayed in Fig. 1(a) and (c), respectively.

To investigate its mechanical behavior at the atomic scale and subpicosecond timescales, uniaxial tensile simulations were performed using the LAMMPS software in MD [38]. The AIREBO-Morse potential function was employed, which effectively models covalent bonding and long-range interactions in carbon-based materials and analogous systems [39]. This potential combines the advantages of the AIREBO potential with Morse terms to describe interatomic interactions. The AIREBO potential function has been extensively used to simulate the mechanical behavior of two-dimensional carbon nanomaterials [14,19], and its reliability and applicability have been well validated by numerous publications (see, for example, Refs. [1–3] and the extensive body of work they cite). In this study, we employed the AIREBO potential to simulate the Net-C18 carbon net structure, following established practice within the field. A cutoff distance of 0.2 nm of C—C bonds was adopted to prevent strain hardening during rapid fracture [40–47].

2.2. MD parameterization and convergence analysis

Three-dimensional periodic boundary constraints were implemented in the in-plane lattice vectors (x/y axes) except for the out-of-plane direction (z-axis), where kinematic freedom was preserved to accommodate uniaxial deformation under multiaxial stress states. Atomic trajectories were propagated using the velocity-Verlet time integration scheme ($\Delta t = 0.0001$ ps) to ensure numerical stability in solving Newtonian dynamics. The energetic minimization protocol was performed through a truncated Newtonian optimizer (conjugate gradient variant), subsequently subjected to isothermal-isobaric (NPT) ensemble equilibration over 40 ps to mitigate lattice distortions and stabilize configurational entropy before mechanical loading. The primary purpose was to

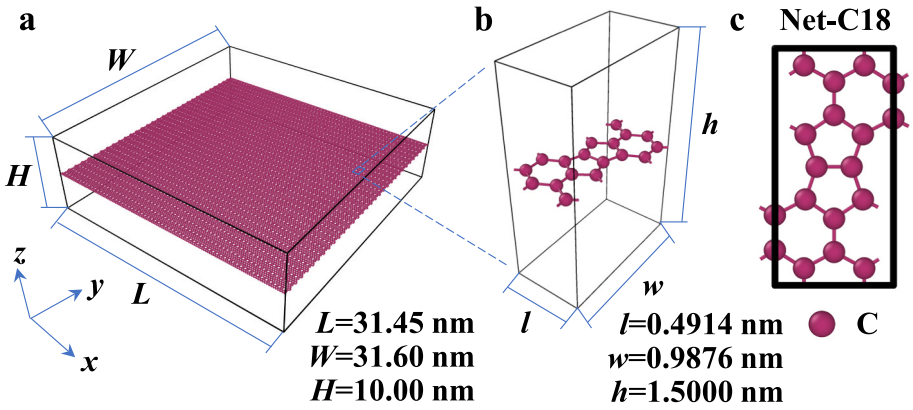

Fig. 1. Structural configuration of single layer Net-C18 model. (a) tilt-view of the full model (supercell) of Net-C18 in this study. The super cell contains 64 × 32×1 unit-cells. The length (L), width (W), and Hight (H) of the supercell is L = 31.45 nm, W = 31.60 nm, and H = 10.00 nm, respectively. The model has 36,864 carbon atoms in total. (b) a 3D unit cell of Net-C18 crystal. The unit-cell contains 18 carbon atoms. The length (l), width (w), and Hight (h) of the unit cell is l = 0.4914 nm, w = 0.9876 nm, h = 1.5000 nm. (c) top-view (xy-plane projection) of the unit cell of (b).

thoroughly eliminate the initial residual stresses within the system at the target temperature (300 K) and zero pressure conditions, allowing the lattice to reach a state of thermodynamic equilibrium. This provides a stable and reliable initial structure for the subsequent tensile simulation.

For tensile simulations, the canonical ensemble (NVT ensemble) was used along the tensile direction. This allows us to precisely control the applied strain rate and achieve quasi-static tensile deformation of the material. Along the transverse direction of the in-plane, the NPT ensemble (with pressure set to zero) was applied. This enables free relaxation (volume change) of the material in the two dimensions perpendicular to the tensile direction during stretching. This releases the stresses generated transversely due to uniaxial tension, more realistically simulating the material's mechanical response under uniaxial tensile loading.

This stage-dependent and direction-specific combination of ensembles (NPT for initial equilibration and transverse stress relaxation, NVT for controlling tensile strain) is a commonly used and justified approach for studying the uniaxial tensile behavior of materials. It ensures the physical soundness of the simulation conditions and the reliability of the results.

Table 1 summarizes the simulation parameters. The initial temperature was set to 300 K, with a simulation duration of 40 ps and an initial strain rate of 10^9/s. Additional parameters, including interatomic force constants and simulation domain dimensions, are provided.

Timestep convergence tests (Δt = 0.0001–0.001 ps) show <2 % deviation in stress. Simulations with varying model sizes (i.e., different numbers of atoms) had been carried out. For defect-free models, deviations in results were within 3 % and negligible when the system exceeded 9216 atoms. In defective models, simulations with 36,864 atoms showed discrepancies of less than 3 % compared to those with 147,456 atoms.

Table 1
Initial parameter settings for LAMMPS computations.

Parameter name	Value	Unit
Size of box	31.45 × 31.60 × 10.00	nm
Size of a single unit cell	0.4914 × 0.9876 × 0.3340	nm
Number of atoms	18 × (64 × 32 × 1)	
Temperature	300	K
Timestep	0.0001	ps
Pair style	airebo/morse	
Cut-off radius	0.30	nm
rc_{min_CC}	0.20	nm
Strain rate	0.0001	1/ps
Relaxation time	40	ps

2.3. Energy equilibration and post-processing

Post-processing and visualization were conducted using OVITO software [50]. In the visualized atomic configurations (Fig. 2), atomic velocities are color-coded, with red and blue representing high and low velocities, respectively. Engineering strain (continuum) is calculated via box dimensions for the stress-strain relationship.

The investigation prioritized (1) nonlinear mechanical response profiles (stress-strain relationships), (2) critical failure thresholds (ultimate strength), (3) elastic stiffness coefficients (Young's modulus), and (4) atomic-scale fracture evolution at femtosecond resolution. Key metrics were derived from stress-strain profiles: ultimate strength corresponds to the peak stress value, fracture strength is the stress at failure, Young's modulus was quantified as the derivative of linear stress-strain proportionality (engineering strain <4 %), while fracture toughness was derived from the total energy dissipation capacity by integrating the area beneath the stress-strain profile until fracture.

3. Results and discussion

3.1. Temperature effects

Thermal conditions serve as a pivotal determinant of material mechanical behavior. For reliable deployment of two-dimensional systems under extreme thermal loads, systematic evaluation of temperature-governed mechanical responses becomes indispensable. As shown in Fig. 3, the temperature-modulated mechanical characteristics of Net-C18—including Young's modulus, failure strength, fracture strain, and fracture toughness with temperature.

Under ambient conditions (300 K), Net-C18 achieves an elastic stiffness of ~948.5 GPa with a critical fracture strain of ~0.19, rivalling that of defect-free graphene in both elastic rigidity and structural robustness [13]. Progressive thermal softening reduces the elastic modulus and ultimate tensile strength to 911.7 GPa and 1.0 GPa at elevated temperatures (900 K), respectively. On one hand, elevated temperatures amplify thermal vibrations of carbon bonds, reducing elastic stiffness. On the other hand, enhanced atomic thermal motion at higher temperatures increases defect nucleation probabilities, degrading plasticity and thereby lowering fracture strain. Similar to graphene, Net-C18 retains superior mechanical properties at high temperatures, albeit with reduced stiffness and toughness relative to room-temperature performance. Overall, the temperature dependence of Net-C18's mechanical properties follows an approximately linear trend.

Notably, fracture in Net-C18 remains fully brittle at temperatures ≤500 K, as evidenced by the absence of discernible nonlinear fracture

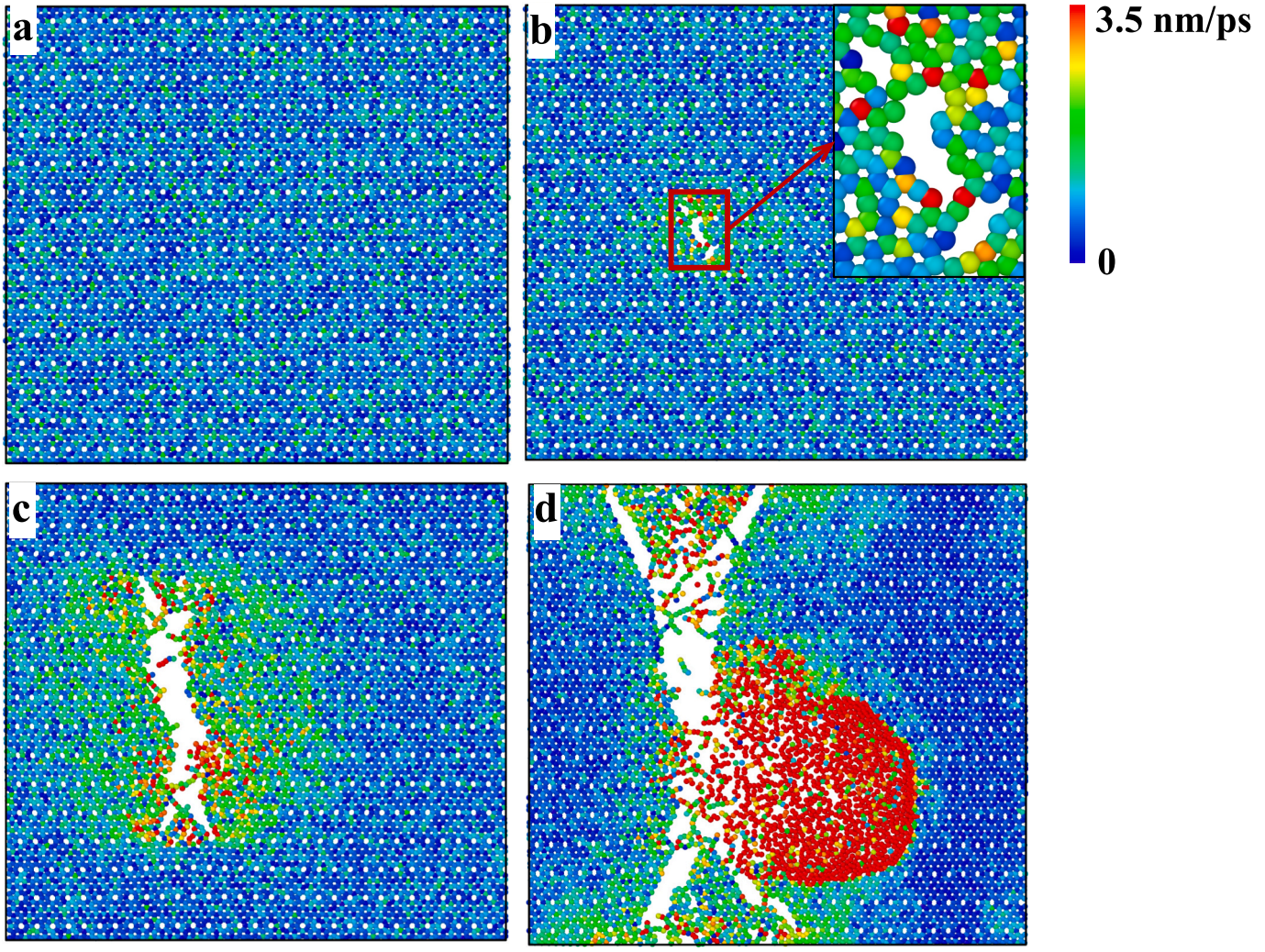

Fig. 2. Atomic velocity vector colormap during tensile deformation. (a) Initial state of the whole system. (b) Micro-crack formation. The inset shows the configurations of the initial microcrack. (c) Crack propagation in the system. (d) Fracture of the system. The atoms are color-coded with the atomistic velocities.

onset phenomena [16] in stress-strain curves near failure. However, ductile behavior emerges at 700 K, where the strain corresponding to peak stress precedes total failure strain. This ductile characteristic becomes pronounced at 900 K (Fig. 4).

3.2. Strain rate effects

D simulations are inherently limited by temporal constraints, resulting in strain rates exceeding experimental values by multiple orders of magnitude. This discrepancy can induce non-equilibrium effects by preventing complete structural relaxation at ultrahigh strain rates, thereby compromising the accuracy of material behavior representation. Moreover, strain rate fundamentally governs deformation mechanisms as materials require finite time to activate stress-responsive processes. Critical mechanisms including dislocation dynamics and crack evolution may remain underdeveloped under accelerated loading conditions compared to quasi-static scenarios. To mitigate these effects, we systematically examined six strain rates (1×10^8/s to 5×10^{10}/s) for tensile characterization, consistent with established protocols for 2D carbon systems.

Fig. 5 compares tensile responses under strain rates varying over three orders of magnitude. The mechanical parameters demonstrate a complex dependence on strain rate, particularly fracture toughness and ultimate strength which exhibit oscillatory characteristics in Fig. 5(b). This non-monotonic behavior implies competing mechanisms in the underlying deformation physics during strain-rate-dependent mechanical evaluations. As illustrated in Fig. 5(c), Young's modulus displays a slight overall increase with rising strain rates, potentially attributable to artifacts arising from incomplete relaxation at high strain rates. Consequently, a strain rate of 1×10^9/s was selected for subsequent simulations, as it induces errors in mechanical property parameters within 5 % compared to lower strain rates.

Compared with other graphene-like materials, Net-C18 demonstrates more noticeable strain rate sensitivity in mechanical properties, though less pronounced than the nanoscale effects observed in metallic nanomaterials or carbon nanotubes. Fig. 5(d) highlights the strain rate dependence of four mechanical properties through five distinct strain rate simulations, with variability ranges of 0.047 and 0.092 observed in fracture strain and failure strength, respectively, while Young's modulus demonstrated negligible variation (0.013). This indicates that strain rate exerts relatively minor effects on Net-C18's mechanical properties compared to factors like temperature and defects, primarily influencing large-strain regions in simulations. The fracture strain variability of 0.047 of Net-C18 is a litter larger than that of graphene (0.03) [19]. This trend aligns with studies on other two-dimensional carbon materials, confirming the strain rate stability of Net-C18's mechanical performance.

While the strain rates employed in MD simulations (10^8/s to 10^{10}/s) exceed experimental values, previous studies on graphene nanoribbons [51] suggest that mechanical responses exhibit a consistent trend across

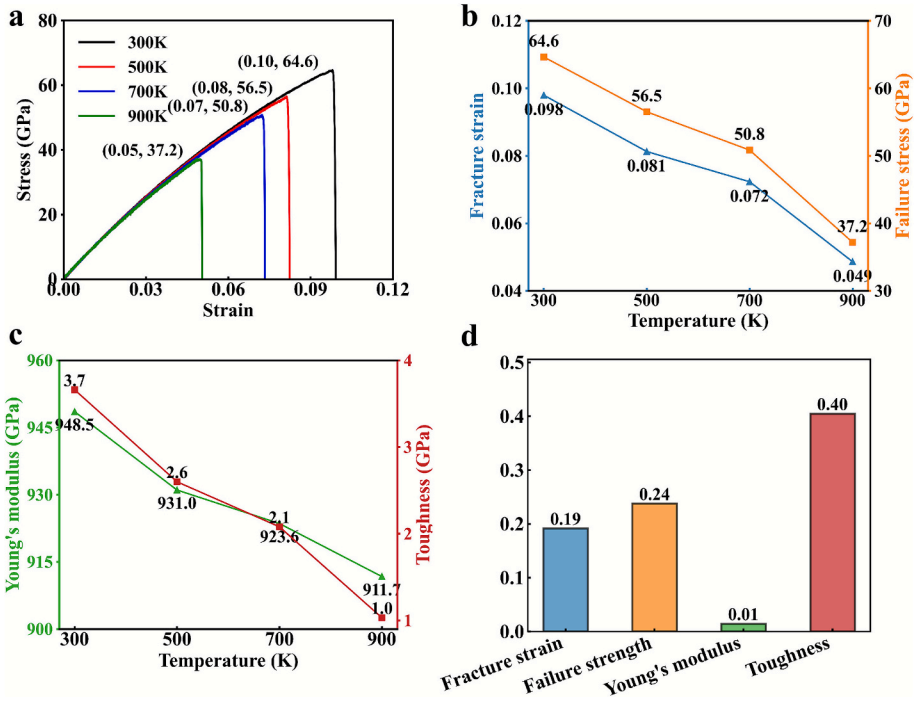

Fig. 3. X-axis tensile tests of Net-C18 at varying temperatures. (a) Stress-strain curves; (b, c) relationships between key mechanical properties and temperature; (d) variations in mechanical properties.

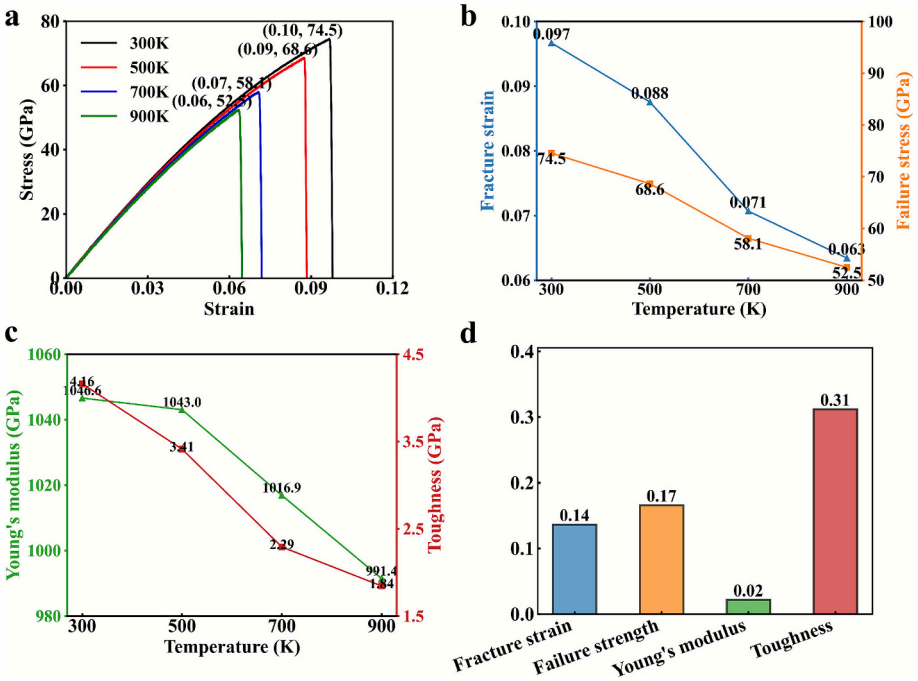

Fig. 4. Temperature-dependent uniaxial tensile responses of Net—C18. (a) Stress-strain profiles; (b, c) thermomechanical coupling of critical mechanical properties; (d) property dispersion analysis.

multiple orders of magnitude. This study assumes that similar scaling effects apply to Net—C18, warranting further experimental validation.

3.3. Crack effects

Pre-existing cracks play a pivotal role in governing material mechanical behavior. Under real-world conditions, fracture initiation predominantly occurs through microcrack tip propagation, contrasting with atomic de-cohesion processes in defect-free crystalline structures. This mechanistic understanding establishes pre-existing flaws as deterministic factors in controlling ultimate failure strength.

Fracture toughness was evaluated by integrating the area beneath the stress-strain curve up to the failure point. The Griffith criterion was employed to estimate the critical energy release rate, which determines the resistance of Net-C18 to crack propagation. According to the Griffith formula [52],

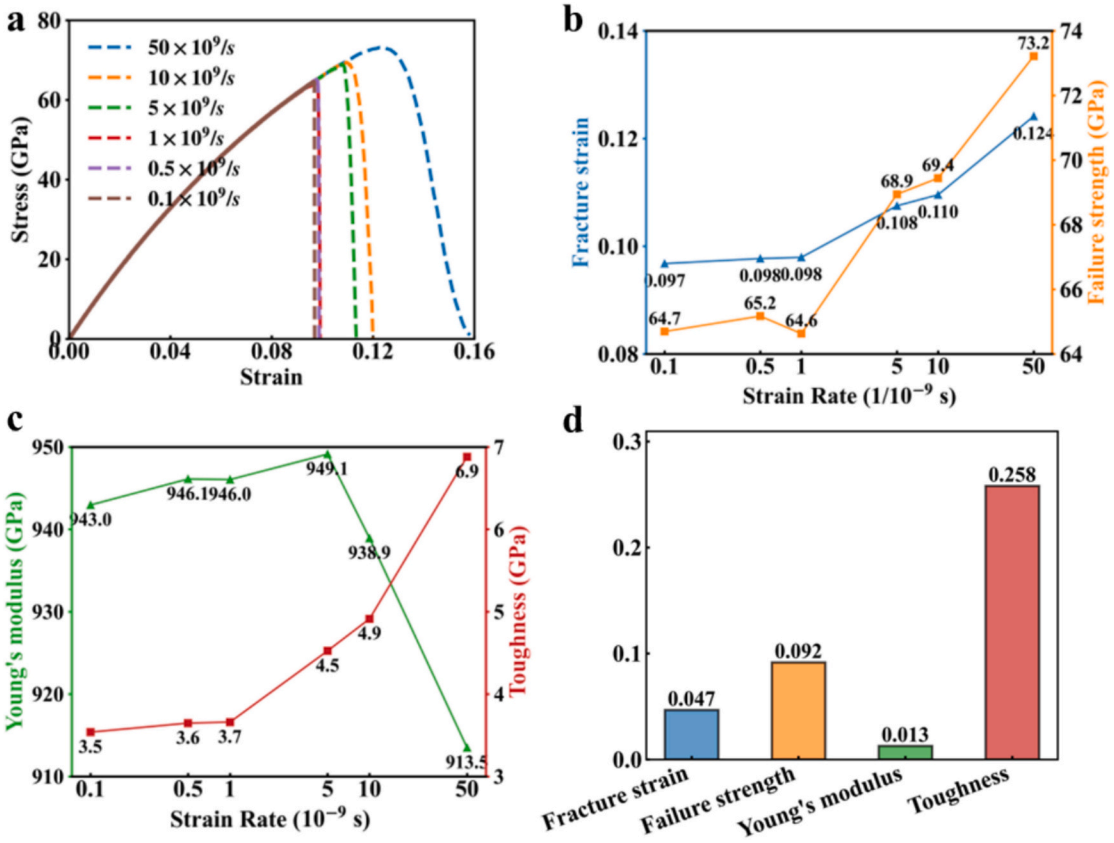

Fig. 5. Tensile tests of Net-C18 under varying strain rates. (a) Stress-strain profiles; (b, c) thermomechanical coupling of critical mechanical properties; (d) property dispersion analysis.

$$\sigma_c = \sqrt{\frac{2Y_s E}{\pi a}} \tag{1}$$

surface energy (Y_s) and crack radius (a) exhibit pronounced effects on tensile failure strength. Crack propagation commences once the crack-tip stress concentration attains the critical bond rupture energy

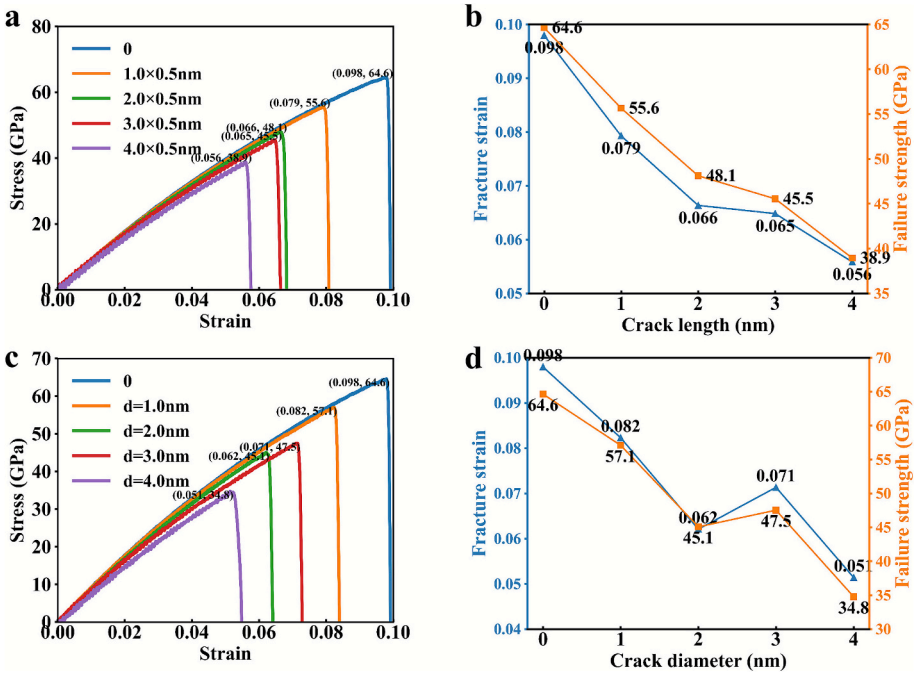

Fig. 6. Tensile tests with holes. (a) Stress-strain curves with square holes, (b) fracture strain and failure strength square holes, (c) stress-strain curves with round holes, (d) fracture strain and failure strength with round holes.

threshold. Furthermore, localized atomic bonding configurations at crack tips govern fracture mechanisms, whereas temperature significantly modulates both crack nucleation kinetics and growth dynamics. To address these interdependencies, we systematically evaluated Net-C18's mechanical response to synergistic thermo-mechanical effects. The computational framework employs pre-engineered flaw geometries with a constant width (0.5 nm) and controlled length parameters (1.0–4.0 nm). It is worth noting that the Griffith criterion was employed solely for qualitative analysis, the validity of Griffith formula at atomic scale is still under debate.

Fig. 6 delineates crack-length-dependent mechanical degradation in Net—C18, a carbon-based graphene structure. Progressive crack extension substantially compromises structural integrity, with fracture strain and failure strength exhibiting proportional reductions as crack length increases. The mechanical response demonstrates non-linear functional dependence on flaw dimensions, manifesting oscillatory decay characteristics superimposed on an overall descending trajectory. This phenomenon originates from dynamic bond reconfiguration processes localized at crack peripheries (Figs. 7, 8).

3.4. Random vacancy defects

Vacancy defects are among the most prevalent defects in crystalline materials. In 2D carbon allotropes, atomic-scale defects emerge through synthesis protocols or irradiation-induced displacement cascades. Such topological defects enable targeted property engineering for functional applications, albeit with inherent mechanical performance trade-offs. Previous studies on graphene have shown that increasing vacancy concentrations lead to a sharp decline in tensile strength and elastic modulus, with clustering effects further exacerbating mechanical degradation [21]. This study extends such analyses to Net—C18, evaluating its unique defect tolerance due to its non-benzenoid atomic structure. To systematically probe vacancy-induced mechanical alterations in Net—C18, a controlled atom removal protocol was implemented across six defect concentrations (0.01–5.00 %) within a 10,000-atom supercell, employing probabilistic removal algorithms to mimic natural defect distributions.

Fig. 9 elucidates vacancy-mediated mechanical degradation in Net—C18. Critical mechanical parameters (fracture strain and failure strength) demonstrate concentration-dependent deterioration, with Net-C18 displaying enhanced defect tolerance relative to benchmark 2D carbon systems. At 1 % vacancy density, Net-C18 maintains 61 % of its intrinsic failure strength, approaching graphene's 69 % strength retention under identical defect conditions. This anomalous behavior arises from structural topology: The quasi-1D carbon chain motifs in Net-C18 permit defect-induced dangling chains to establish transient covalent interactions with neighboring atoms under strain, effectively redistributing stress concentrations and maintaining structural integrity approaching defect-free graphene.

Furthermore, real-world spatial arrangements of crystalline defects often diverge from computational probabilistic defect generation protocols. These topological mismatches may induce non-uniform mechanical outcomes under vacancy loading scenarios, necessitating advanced characterization methodologies for experimental validation.

3.5. Analytic model

To further analyze the temperature and strain rate dependence of Net-C18's fracture behavior, we integrated the Arrhenius equation with Bailey's durability criterion into our computational framework. This approach has been successfully applied to model defective graphene systems [48], and here we extend it to Net-C18 while acknowledging the absence of free edge effects in the current formulation.

The Bailey's criterion provides a phenomenological basis for estimating material lifetime under thermomechanical loads [49], expressed as:

$$\int_0^{t_f} \frac{dt}{\tau(T,t)} = 1 \tag{2}$$

where t_f is the time to fracture, and $\tau(T,t)$ is the temperature-dependent durability function derived from experimental or simulated data. The relationship between reaction rate constant R and temperature T can be described with the Arrhenius equation:

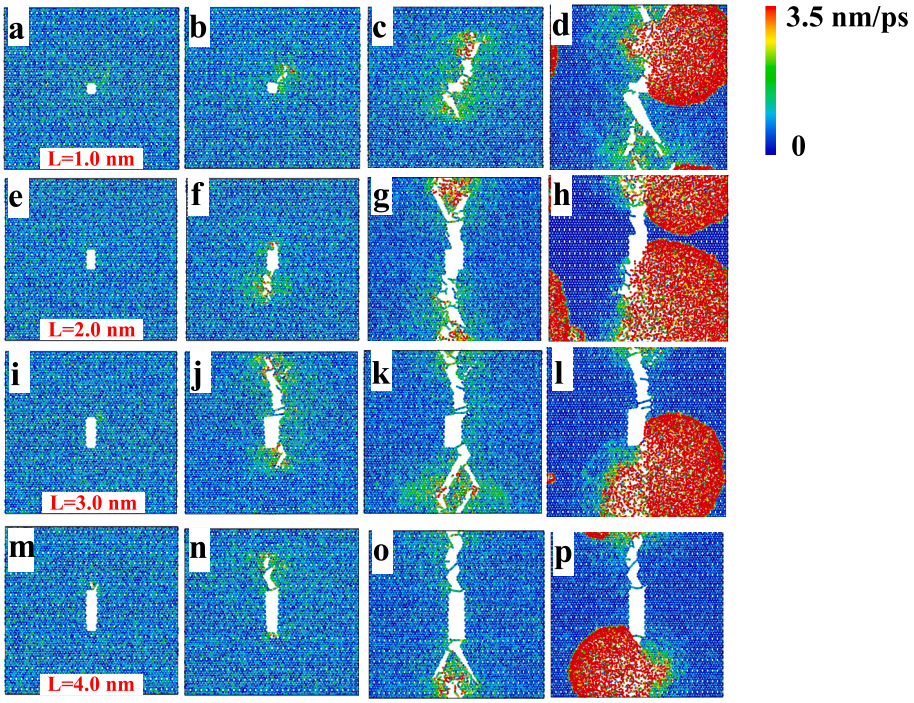

Fig. 7. Crack propagation during tensile loading with square holes. (a, b, c, d) L = 1.0 nm; (e, f, g, h) L = 2.0 nm; (i, j, k, l) L = 3.0 nm; (m, n, o, p) L = 4.0 nm.

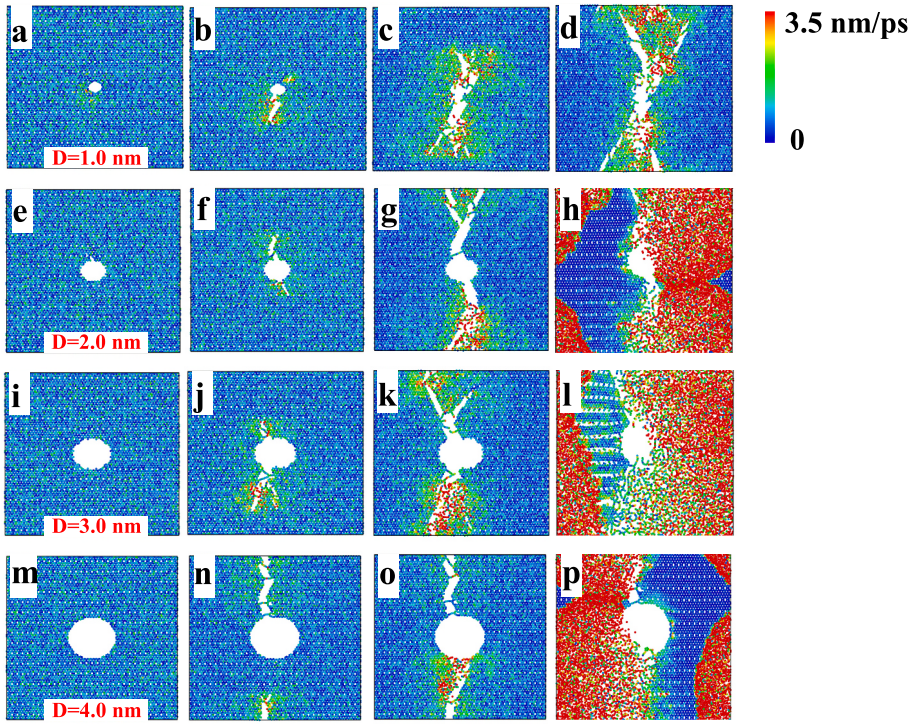

Fig. 8. Crack propagation during tensile loading with round holes. (a, b, c, d) D = 1.0 nm; (e, f, g, h) D = 2.0 nm; (i, j, k, l) D = 3.0 nm; (m, n, o, p) D = 4.0 nm.

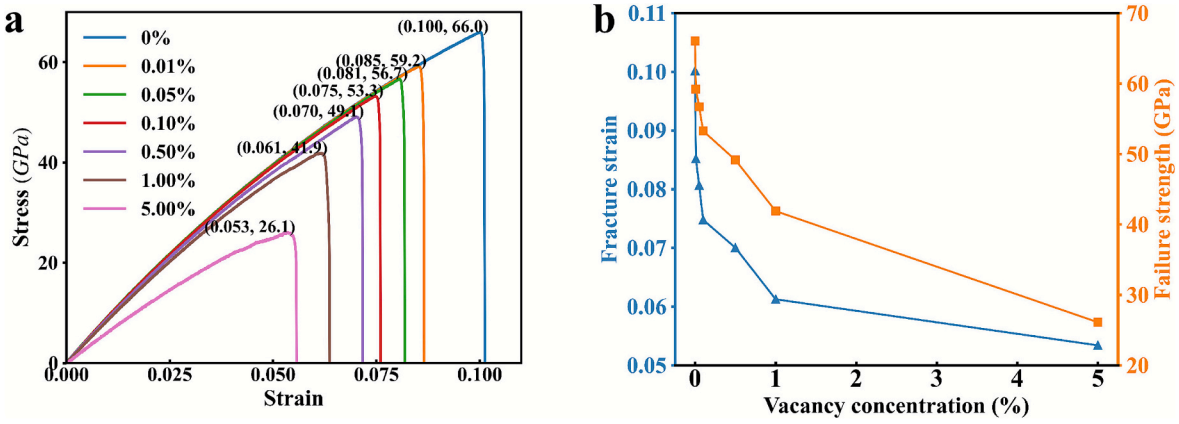

Fig. 9. Tensile tests with vacancy. (a) Stress-strain curves, (b) fracture strain and failure strength.

$$R = \tau_0 \exp\left(\frac{\boldsymbol{E_a}}{\boldsymbol{k_B} T}\right) \tag{3}$$

where $\boldsymbol{E_a}$ is the activation energy for bond rupture and $\boldsymbol{k_B}$ is the Boltzmann constant.

By substituting the Arrhenius-type expression for the durability function $\tau(T,t)$ into Bailey's integral criterion, we establish a temperature- and time-dependent framework to predict fracture time t_f with enhanced physical fidelity [53]. This integration allows us to systematically capture the thermally activated failure processes in Net-C18 under various loading conditions. The durability function of net-C18 is defined as:

$$\tau(T,t) = \frac{\tau_0}{n} \exp\left(\frac{\boldsymbol{E_a}(t)}{C\boldsymbol{k_B} T}\right) \tag{4}$$

where τ_0 is the vibration period of carbon atoms of Net—C18, with a value of 0.005 ps [54], n represents the number of bonds in the sheet, $\boldsymbol{E_a}$ is the activation energy for bond breaking, $\boldsymbol{k_B}$ is the Boltzmann constant, and C is a correction factor set to 1.7. T denotes the temperature. This model quantifies defect-mediated fracture dynamics [55]. For Net—C18, we calibrated $\tau(T)$ using MD-derived stress relaxation data from 300 to 900 K to capture its unique bond reconstruction dynamics. The specific formula for $\boldsymbol{E_a}$ is as follows:

$$\boldsymbol{E_a}(t) = \frac{U_0}{\beta} - \gamma\sigma(t) \tag{5}$$

where U_0 is the bond dissociation energy between carbon atoms, which is 4.362 eV [56]. γ=νq, where ν is the activation volume, set to 9.0 Å^3, and q is the directional constant, which is 1 in this case. β represents the reduction in the average bond dissociation energy due to the presence of vacancies and is defined as follows:

$$\beta = \begin{cases} 1, & \alpha = 0 \\ p\alpha + k, & \alpha > 0 \end{cases} \tag{6}$$

where α represents the vacancy percentage. p denotes the reduction rate

due to the increase in vacancies, with a value of 0.25. k represents the strength reduction of the material when only a single vacancy is present, with a value of 1.1. $\sigma(t)$ is a function of time t and can be expressed as:

$$\sigma(t) = a(\dot{\varepsilon}t) + b(\dot{\varepsilon}t)^2 \tag{7}$$

where a and b are obtained from the stress-strain curve in the MD simulation, with values of 925.9 GPa and 2721.9 GPa, respectively. This model enables quantification of defect-mediated fracture kinetics.

The model calculates $\tau(T, t)$, then substitutes τ into Eq. (1) to solve for t_f. t_f is then substituted into Eq. (7) to obtain the predicted ultimate stress $\sigma(t_f)$. Fig. 10 illustrates the predicted ultimate stress of Net-C18 at different temperatures, while Fig. 11 presents the predicted ultimate stress of Net-C18 for various defect ratios.

Fig. 10 shows that the computational model aligns well with the MD results. Across different temperatures, the maximum prediction error does not exceed 10 %, indicating that the model effectively captures the key characteristics of the system. Since the chemical bonds in Net-C18 are sp^2 hybridized, closely resembling those in graphene, this model can be extended to Net-C18 for predicting strength at different temperatures.

As shown in Fig. 11, the computational model also provides accurate strength predictions for defective Net—C18. Except for the 5 % defect ratio, the maximum error between the predictions and MD simulations does not exceed 6 %. However, when the defect ratio increases to 5 %, the model's predictions become inaccurate, possibly due to structural changes in Net-C18 under such defect conditions. Overall, compared to MD simulations, using this analytical model for strength prediction of defective Net-C18 is more efficient and straightforward.

It is worth noting that the Net-C18 structure investigated in this work is a computationally designed, predictive material that has not yet been experimentally synthesized. We attempt to have a conceptual discussion regarding its potential experimental preparation pathways and emphasized the significant challenges involved.

First, we first emphasize that Net-C18 is a computationally predicted structure and highlight the substantial challenges its experimental synthesis would face. These include the precise control required for forming the sp-sp^2 hybridized carbon atom network, managing the stability of the high-density ethynylene bridges (-C≡C-), and achieving the atomically precise periodic pore structure.

Second, although no direct method for synthesizing Net-C18 has been reported to date, we discuss possible strategic directions inspired by current techniques for synthesizing and modifying advanced carbon materials (such as graphene, carbyne chains, and graphdiyne derivatives):

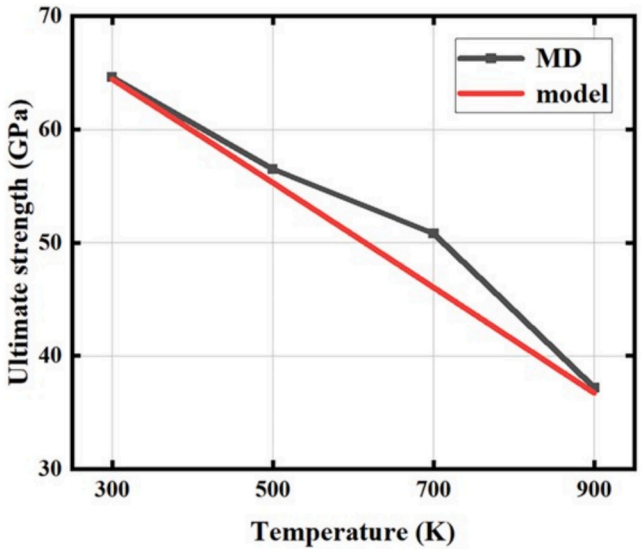

Fig. 10. Comparison of the model-predicted strength of Net-C18 at different temperatures with MD simulation results, at temperatures of 300 K, 500 K, 700 K, and 900 K.

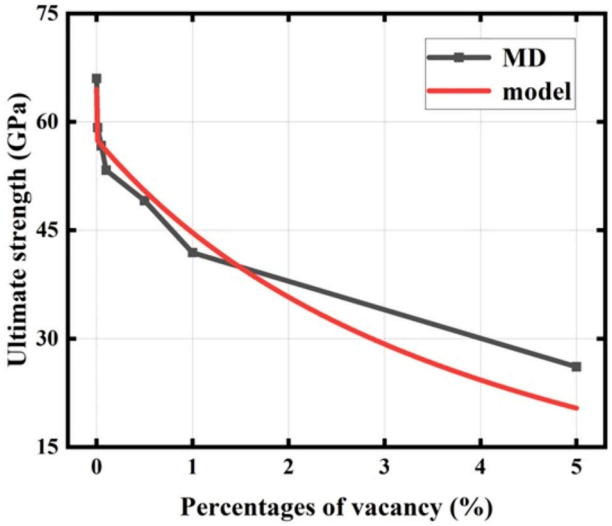

Fig. 11. Compare the strength of the defect Net-C18 predicted by the model with the MD simulation results, with defect rates of 0 %, 0.01 %, 0.05 %, 0.1 %, 0.5 %, 1.0 %, and 5.0 %.

Precision Etching/Patterning Strategy: Drawing inspiration from techniques like scanning probe microscopy (SPM) or electron-beam-induced chemical reactions used for atomic-precision etching and patterning on substrates like graphene (e.g., the work by Cai et al., Ref. [8]), it is theoretically conceivable that Net-C18's pore and chain structure could be "sculpted" onto a specific carbon substrate with extremely precise control. However, this would demand unprecedented levels of precision and stability.

Directed Bottom-Up Assembly: Inspired by the precise synthesis of complex carbon nanostructures via surface synthesis or solution chemistry (e.g., the synthesis of graphdiyne derivatives [57]), we envision the potential of designing specific molecular precursors and employing controlled, multi-step dehydrocyclization or coupling reactions to progressively build the Net-C18 framework. This approach also faces immense challenges, such as intermediate stability, reaction selectivity, and regiocontrol.

At last, we clearly state that these synthesis concepts remain highly conceptual and exploratory at this stage. Their practical feasibility necessitates significant future breakthroughs in experimental methodology for validation. Our primary aim is to theoretically elucidate the exceptional mechanical properties of Net—C18, thereby providing a theoretical foundation and target direction for its future experimental exploration.

4. Conclusion

This investigation implemented MD simulations to systematically probe thermo-mechanical coupling effects, strain rate, cracks, and defect sensitivity in Net—C18. Strain rate dependencies reveal the absence of statistically significant correlations with tensile characteristics under quasi-static loading regimes. Crucially, ultrahigh loading rates ($>10^8$/s) generate non-equilibrium dynamic artifacts, resulting in artificially elevated Young's modulus at extreme strains and compromised accuracy in strength/strain failure predictions. Thermal analyses demonstrate a 50 % reduction in ultimate failure stress across the 300–900 K range, accompanied by temperature-dependent failure mode transitions where nonlinear fracture onset supersedes brittle fracture at elevated temperatures. Notably, Net-C18 exhibits enhanced defect

tolerance versus reference carbon allotropes under equivalent vacancy concentrations. These behaviors are attributed to its intrinsic elongated carbon chain structure, which enables unsaturated carbon atoms at defect sites to form new chemical bonds under tension, compensating for strength loss. Net-C18's 61 % strength retention at 1 % vacancies (vs. graphene's 69 %) due to quasi-1D chain self-healing –a topology-dependent mechanism unreported elsewhere. The results also reveal that pre-existing cracks substantially degrade Net-C18's mechanical performance. Our findings provide atomic-scale mechanistic insights into the mechanical behavior of Net-C18 under diverse external parameters and offer valuable guidance for its design and application in flexible electronic devices.

CRediT authorship contribution statement

Xintian Cai: Writing – review & editing, Writing – original draft, Visualization, Validation, Project administration, Methodology, Investigation, Formal analysis, Data curation, Conceptualization. **Ao Li:** Visualization, Software. **Xue Chen:** Validation, Software. **Zeyu Huang:** Software, Methodology, Investigation. **Gen Chen:** Software. **Chaoyue Ji:** Software, Investigation. **Han Yan:** Validation, Supervision. **Xiao-Jia Chen:** Resources, Funding acquisition. **Qing Peng:** Validation, Supervision, Software, Resources, Project administration, Methodology, Investigation, Funding acquisition, Formal analysis, Data curation, Conceptualization.

Declaration of competing interest

The authors declare that they have no known competing financial interests or personal relationships that could have appeared to influence the work reported in this paper.

Acknowledgements

This research was funded by the Shenzhen Science and Technology Program (Grant No. KQTD20200820113045081), Educational Commission of Hubei Province of China (Grant No. Q20233005), Doctoral Research Initiation Fund of Hubei University of Technology (grant No. XJ2024008301), Strategic Priority Research Program of Chinese Academy of Sciences (Grant No. XDB0620103), National Natural Science Foundation of China (Grant No. 12272378).

Data availability

The raw/processed data required to reproduce the findings in the current manuscript cannot be shared at this time, as these data also form part of an ongoing study.

References

[1] H.P. Boehm, R. Setton, E. Stumpp, Nomenclature and terminology of graphite intercalation compounds, Carbon 24 (2) (1986) 241–245.
[2] K.S. Novoselov, A.K. Geim, S.V. Morozov, D.E. Jiang, Y. Zhang, S.V. Dubonos, A. A. Firsov, Electric field effect in atomically thin carbon films, Science 306 (5696) (2004) 666–669.
[3] A.K. Geim, Graphene: status and prospects, Science 324 (5934) (2009) 1530–1534.
[4] M. Xu, T. Liang, M. Shi, H. Chen, Graphene-like two-dimensional materials, Chem. Rev. 113 (5) (2013) 3766–3798.
[5] B. Mortazavi, M. Shahrokhi, M. Raeisi, X. Zhuang, L.F.C. Pereira, T. Rabczuk, Outstanding strength, optical characteristics and thermal conductivity of graphene-like BC3 and BC6N semiconductors, Carbon 149 (2019) 733–742.
[6] H. Xiao, J. Lv, X. Zhao, X. He, M. Chen, W. Tan, G. Yang, Multiscale lamellar regulation of three-dimensional graphene-like nanostructures for electromagnetic interference shielding and thermal management, ACS Appl. Nano Mater. 7 (13) (2024) 15583–15592.
[7] S. Peng, W. Chen, L. Fan, H. Zheng, X. Guo, P. Zheng, Y. Zhang, The preparation and properties of in situ grown oriented nitrogen-doped graphene-like/copper composite materials, ACS Appl. Electron. Mater. 6 (2) (2024) 1396–1404.
[8] X.H. Cai, Q. Yang, S. Zheng, M. Wang, Net-C18: a predicted two-dimensional planar carbon allotrope and potential for an anode in lithium-ion battery, Energy Environ. Mater. 4 (3) (2021) 458–464.
[9] B.I. Kharisov, O.V. Kharissova, L.T. González, Y. Peña Méndez, I.E. Uflyand, N. Kulkarni, Density function theory predicted carbon allotropes: recent developments, ChemistrySelect 8 (24) (2023) e202301567.
[10] A.K. Geim, K.S. Novoselov, The rise of graphene, Nat. Mater. 6 (3) (2007) 183–191.
[11] C. Lee, X. Wei, J.W. Kysar, J. Hone, Measurement of the elastic properties and intrinsic strength of monolayer graphene, Science 321 (5887) (2008) 385–388.
[12] F. Memarian, A. Fereidoon, M.D. Ganji, Graphene young's modulus: molecular mechanics and DFT treatments, Superlattice. Microst. 85 (2015) 348–356.
[13] R. Faccio, P. Denis, H. Pardo, C. Goyenola, A. Mombru, Investigation on the mechanical properties and fracture phenomenon of silicon doped graphene by molecular dynamics simulation, RSC Adv. 10 (60) (2020) 36514–36522.
[14] Q. Peng, C. Liang, W. Ji, S. De, A first principles investigation of the mechanical properties of g-ZnO: the graphene-like hexagonal zinc oxide monolayer, Comput. Mater. Sci. 68 (2013) 320–324.
[15] Q. Peng, X.J. Chen, S. Liu, S. De, Mechanical stabilities and properties of graphene-like aluminum nitride predicted from first-principles calculations, RSC Adv. 3 (19) (2013) 7083–7092.
[16] D.A. Damasceno, R.K.N.D. Rajapakse, E. Mesquita, R. Pavanello, Atomistic simulation of tensile strength properties of graphene with complex vacancy and topological defects, Comput. Mater. Sci. 153 (2018) 493–502.
[17] B. Mortazavi, S. Ahzi, Thermal conductivity and tensile response of defective graphene: a molecular dynamics study, Carbon 63 (2013) 460–470.
[18] L.R. Safina, K.A. Krylova, J.A. Baimova, Molecular dynamics study of the mechanical properties and deformation behavior of graphene/metal composites, Mater. Today Phys. 28 (2022) 100851.
[19] T. Zhang, X. Li, H. Gao, Fracture of graphene: a review, Int. J. Fract. 196 (2015) 1–31.
[20] P. Bhauriyal, A. Mahata, B. Pathak, Graphene-like carbon–nitride monolayer: a potential anode material for Na-and K-ion batteries, J. Phys. Chem. C 122 (5) (2018) 2481–2489.
[21] Y. Kumar, S. Sahoo, A.K. Chakraborty, Mechanical properties of graphene, defective graphene, multilayer graphene and SiC-graphene composites: a molecular dynamics study, Phys. B Condens. Matter 620 (2021) 413250.
[22] A. Santonocito, B. Patrizi, G. Toci, Recent advances in tunable metasurfaces and their application in optics, Nanomaterials 13 (10) (2023) 1633.
[23] Y. Yang, J. Cao, N. Wei, D. Meng, L. Wang, G. Ren, N. Zhang, Thermal conductivity of defective graphene oxide: a molecular dynamic study, Molecules 24 (6) (2019) 1103.
[24] B. Anegbe, I.H. Ifijen, M. Maliki, I.E. Uwidia, A.I. Aigbodion, Graphene oxide synthesis and applications in emerging contaminant removal: a comprehensive review, Environ. Sci. Eur. 36 (1) (2024) 15.
[25] I.F. Akyildiz, C. Han, Z. Hu, S. Nie, J.M. Jornet, Terahertz band communication: an old problem revisited and research directions for the next decade, IEEE Trans. Commun. 70 (6) (2022) 4250–4285.
[26] M.A. Rozhkov, A. Kolesnikova, A. Romanov, Comparison of interatomic potentials for modeling defects in graphene using molecular dynamics, Rev. Adv. Mater. Technol. 6 (2024) 35–42.
[27] D.K. Das, B. Kumar, Mechanical properties of aluminium-graphene core shell nanocomposite: a molecular dynamics simulation study, Diam. Relat. Mater. 152 (2025) 111981.
[28] J. Ma, K. Wang, M. Tang, Y. He, X. Gao, P. Gao, J. Sun, Effect of monovacancy defects on anisotropic mechanical behavior of monolayer graphene: a molecular dynamics study, Diam. Relat. Mater. 148 (2024) 111437.
[29] C. Zhao, J. Zhou, K. Zhong, Y. Bai, L. Qi, Enhancing understanding metal matrix composites through molecular dynamics simulation: a comprehensive review, Comput. Mater. Sci. 239 (2024) 112993.
[30] N. Duhan, B. Chakraborty, T.D. Kumar, Biphenylene-graphene van der Waals bilayer heterostructure as an anode material for Li-ion batteries, J. Energy Storage 112 (2025) 115469.
[31] F. Najafi, G. Wang, T. Cui, A. Anand, S. Mukherjee, T. Filleter, C.V. Singh, Fatigue resistance of atomically thin graphene oxide, Carbon 183 (2021) 780–788.
[32] H. Lyu, J. He, C. Wang, X. Jia, K. Li, D. Yan, J.A. Duan, Low-temperature sinterability of graphene-Cu nanoparticles: molecular dynamics simulations and experimental verification, Appl. Surf. Sci. 682 (2025) 161683.
[33] L. Han, X. Zhang, F. Wu, T. Wang, H. Zhai, Exploring the binding mode of BBA protein anchored on defective graphene and evaluating the biocompatibility of two types of graphene with λ-repressor protein, Colloids Surf. B: Biointerfaces 249 (2025) 114510.
[34] L. Mihlan, J. Ehrens, J. Schnack, Comparison of various schemes to determine the Young's modulus of disordered carbon nanomembranes compared to crystalline graphene, Phys. E. 167 (2025) 116170.
[35] L.F.C. Pereira, Investigating mechanical properties and thermal conductivity of 2D carbon-based materials by computational experiments, Comput. Mater. Sci. 196 (2021) 110493.
[36] Q. Bao, Z. Yang, Z. Lu, X. He, Effects of graphene thickness and length distribution on the mechanical properties of graphene networks: a coarse-grained molecular dynamics simulation, Appl. Surf. Sci. 570 (2021) 151023.
[37] R. El Fdil, H. Sabbah, Z. Fadil, C.J. Raorane, E. Salmani, A.A. Alsayyari, H. Ez-Zahraouy, Edge vacancy effects on magnetic behavior in graphene-like nanostructure: Monte Carlo simulations, SPIN (2010-3247) 14 (4) (2024).
[38] S. Plimpton, Fast parallel algorithms for short-range molecular dynamics, J. Comput. Phys. 117 (1) (1995) 1–19.
[39] T.C. O'Connor, J. Andzelm, M.O. Robbins, AIREBO-M: a reactive model for hydrocarbons at extreme pressures, J. Chem. Phys. 142 (2) (2015) 024903.
[40] H. Zhao, K. Min, N.R. Aluru, Size and chirality dependent elastic properties of graphene nanoribbons under uniaxial tension, Nano Lett. 9 (8) (2009) 3012–3015.

https://www.ncbi.nlm.nih.gov/pubmed/19719113. https://doi.org/10.1021/nl901448z.
[41] T. Zhang, X. Li, S. Kadkhodaei, H. Gao, Flaw insensitive fracture in nanocrystalline graphene, Nano Lett. 12 (9) (2012) 4605–4610.
[42] Y. Wei, J. Wu, H. Yin, X. Shi, R. Yang, M. Dresselhaus, The nature of strength enhancement and weakening by pentagon-heptagon defects in graphene, Nat. Mater. 11 (9) (2012) 759–763.
[43] O.A. Shenderova, D.W. Brenner, A. Omeltchenko, X. Su, L.H. Yang, Atomistic modeling of the fracture of polycrystalline diamond, Phys. Rev. B 61 (6) (2000) 3877–3888.
[44] R. Grantab, V.B. Shenoy, R.S. Ruoff, Anomalous strength characteristics of tilt grain boundaries in graphene, Science 330 (6006) (2010) 946–948.
[45] H. Zhao, N.R. Aluru, Temperature and strain-rate dependent fracture strength of graphene, J. Appl. Phys. 108 (6) (2010) 3488620.
[46] Z. Qi, F. Zhao, X. Zhou, Z. Sun, H.S. Park, H. Wu, A molecular simulation analysis of producing monatomic carbon chains by stretching ultranarrow graphene nanoribbons, Nanotechnology 21 (26) (2010) 265702.
[47] Y.I. Jhon, S.-E. Zhu, J.-H. Ahn, M.S. Jhon, The mechanical responses of tilted and non-tilted grain boundaries in graphene, Carbon 50 (10) (2012) 3708–3716.
[48] M.A.N. Dewapriya, R.K.N.D. Rajapakse, Effects of free edges and vacancy defects on the mechanical properties of graphene, in: Paper presented at the 14th IEEE International Conference on Nanotechnology, 2014.
[49] A.D. Freeds, A.I. Leonov, The bailey criterion: statistical derivation and applications to interpretations of durability tests and chemical kinetics, Zeitschrift für angewandte Mathematik und Physik ZAMP 53 (1) (2002) 160–166.
[50] A. Stukowski, Visualization and analysis of atomistic simulation data with OVITO – the Open Visualization Tool, Model. Simul. Mater. Sci. Eng. 18 (1) (2010) 015012.
[51] H. Zhao, K. Min, N.R. Aluru, Size and chirality dependent elastic properties of graphene nanoribbons under uniaxial tension, Nano Lett. 9 (8) (2009) 3012–3015.
[52] A.A. Griffith, The phenomena of rupture and flow in solids, Philos. Trans. Royal Soc. London. Ser. A, Contain. Papers Math. Phys. Char. 221 (582–593) (1921) 163–198.
[53] H. Zhao, N.R. Aluru, Temperature and strain-rate dependent fracture strength of graphene, J. Appl. Phys. 108 (6) (2010).
[54] K. Mylvaganam, L.C. Zhang, Important issues in a molecular dynamics simulation for characterising the mechanical properties of carbon nanotubes, Carbon 42 (10) (2004) 2025–2032.
[55] A.D. McQuarrie, C.L. Tsai, Regression and Time Series Model Selection, World Scientific, 1998.
[56] F. Jensen, Introduction to Computational Chemistry, John Wiley & Sons, 2017.
[57] S.J. Hein, D. Lehnherr, H. Arslan, F.J. Uribe-Rome, W.R. Dichtel, Alkyne benzannulation reactions for the synthesis of novel aromatic architectures, Acc. Chem. Res. 50 (11) (2017) 2776–2788.